Nanoscale

Accepted Manuscript

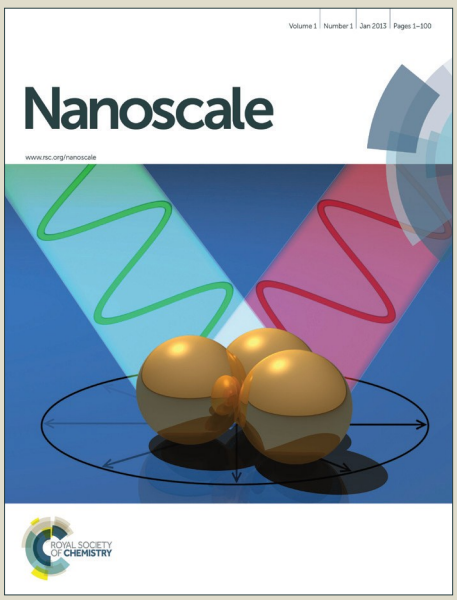

ROYAL SOCIETY OF CHEMISTRY

www.rsc.org/nanoscale

Journal Name

ARTICLE

The mechanical bond on carbon nanotubes: diameter-selective functionalization and effects on physical properties†

Received 00th January 20xx,
Accepted 00th January 20xx

DOI: 10.1039/x0xx00000x

www.rsc.org/

Emiliano Martínez-Periñán[a], Alberto de Juan[b], Yann Pouillon[c], Christoph Schierl[d], Volker Strauss[d], Nazario Martín[b,e], Ángel Rubio[*c], Dirk M. Guldi[*d], Encarnación Lorenzo[*a,b] and Emilio M. Pérez[*b]

We describe the functionalization of SWNTs enriched in (6,5) chirality with electron donating macrocycles to yield rotaxane-type mechanically interlocked carbon nanotubes (MINTs). Investigations by means of electron microscopy and control experiments corroborated the interlocked nature of the MINTs. A comprehensive characterization of the MINTs through UV-vis-NIR, Raman, fluorescence, transient absorption spectroscopy, cyclic voltammetry, and chronoamperometry was carried out. Analyses of the spectroscopic data reveal that the MINT-forming reaction proceeds with diameter selectivity, favoring functionalization of (6,5) SWNTs rather than larger (7,6) SWNTs. In the ground state, we found a lack of significant charge-transfer interactions between the electron donor exTTF and the SWNTs. Upon photoexcitation, efficient charge-transfer between the electron donating exTTF macrocycles and SWNTs was demonstrated. As a complement, we established significantly different charge-transfer rate constants and diffusion coefficients for MINTs and the supramolecular models, which confirms the fundamentally different type of interactions between exTTF and SWNTs in the presence or absence of the mechanical bond. Molecular mechanics and DFT calculations support the experimental findings.

Introduction

Mechanically interlocked molecules (MIMs) feature submolecular components linked together as a consequence of their topology,[1] in the absence of covalent bonds between them. The different constituents of MIMs cannot be detached from one another without breaking a covalent bond.[2] Compared to supramolecular constructs, the fingerprint of the mechanical bond is therefore the absence of equilibrium between associated and dissociated components. In other words, the rate of dissociation in MIMs is 0, so that they can be looked at as supramolecular associates where the binding constant between their components is infinite.[3]

Rotaxanes are a leading example of MIMs, wherein one or more macrocycles are threaded around a linear component (thread) from which they cannot be detached due to the presence of bulky substituents (stoppers) at both ends of the thread.[2] The possibility of moving the macrocycle(s) along the thread in a controlled fashion has attracted a great deal of attention towards rotaxanes as components in artificial molecular machinery.[4-9] Besides their extraordinary dynamic properties, the mechanical bond between macrocycle and thread in rotaxanes often results in a significant influence on their respective properties.[10] For instance, the macrocycle can serve as a noncovalently attached protecting group for the thread,[11-16] or modulate its photophysical properties.[17-21] These observations have motivated the search for mechanically interlocked materials beyond small-molecules, including metal organic frameworks,[22-28] and polymers.[29-37]

One of the main reasons carbon nanotubes continue to attract ever-increasing attention[38-44] is their potential application in the field of organic electronics.[45-49] Any such applications will require a precise modulation of the electronic properties of the nanotubes. To that end, several strategies for the covalent[50-54] or supramolecular[55-58] chemical modification of single wall carbon nanotubes (SWNT) have been developed. The main factor governing SWNT electronic properties is their chirality, but strategies for the noncovalent functionalization of SWNTs in a chirality selective-fashion are scarce.[59-63]

We have recently introduced the mechanical bond as a new tool for the chemical modification of SWNTs. In particular, we described the synthesis of rotaxane-type derivatives of SWNTs – the first example of mechanically interlocked SWNTs (MINTs).[64-66] With synthetic routes towards MINTs established,

[a] Departamento de Química Analítica y Análisis Instrumental, Facultad de Ciencias, Universidad Autónoma de Madrid, C/ Francisco Tomás y Valiente, 7, 28049 Madrid, Spain.
[b] IMDEA Nanoscience, C/Faraday 9, Ciudad Universitaria de Canto Blanco, 28049 Madrid, Spain.
[c] Centro Joxe Mari Korta, Avenida de Tolosa, 72, 20018 Donostia-San Sebastian, Spain.
[d] Friedrich-Alexander-Universität Erlangen/Nürnberg, Department Chemie und Pharmazie, Lehrstuhl für Physikalische Chemie I, Egerlandstraße 3, 91058 Erlangen, Germany.
[e] Departamento de Química Orgánica, Facultad de CC Químicas, Universidad Complutense de Madrid, 28040 Madrid, Spain.

†Electronic Supplementary Information (ESI) available: Synthetic details, experimental procedures, supplementary figures, and complete data set of interaction energies. See DOI: 10.1039/x0xx00000x

we decided to investigate the consequences of the mechanical bond on the properties of both SWNT and macrocycle(s).
Here, we report that the MINT-forming reaction proceeds in a chirality-selective fashion, favoring functionalization of smaller diameter SWNTs. Moreover, the mechanical bond shows distinctive effects on the electronic properties of macrocycles and nanotubes in MINTs. Our conclusions are based on the complete photophysical and electrochemical characterization of MINTs in comparison with pristine nanotubes, and whenever possible, the corresponding supramolecular model compounds. The experimental results are backed up by calculations at the molecular mechanics and DFT levels.

Results and discussion

For all measurements, we have used CoMoCat (6,5) enriched SWNTs. The synthesis of MINTs was carried out with the U-shaped molecule **1**, depicted in Figure 1, which features two units of a π-extended tetrathiafulvalene (exTTF) as recognition motif towards SWNTs.[67,68] The experimental procedures for synthesis and purification have been described previously for other types of SWNTs.[66] Very briefly, we exploited the positive exTTF-SWNT interaction[67] to template the ring closing metathesis of **1** around the nanotubes, to form MINTs (Figure 1). Unreacted **1**, non-threaded **2**, linear oligomers of **1**, formed in situ under the RCM reaction conditions, catalyst, etc. were removed by extensive washing with dichloromethane. The MINT$_{(6,5)}$-**2** samples used in these experiments showed a macrocycle loading of 32% by themogravimetric analysis. The extreme aspect ratio of the nanotubes guarantees the formation of cross-points between them, which act as stoppers and prevent de-threading of **2** in MINTs, even under reflux in tetrachloroethane (see the Supplementary Information).[66]

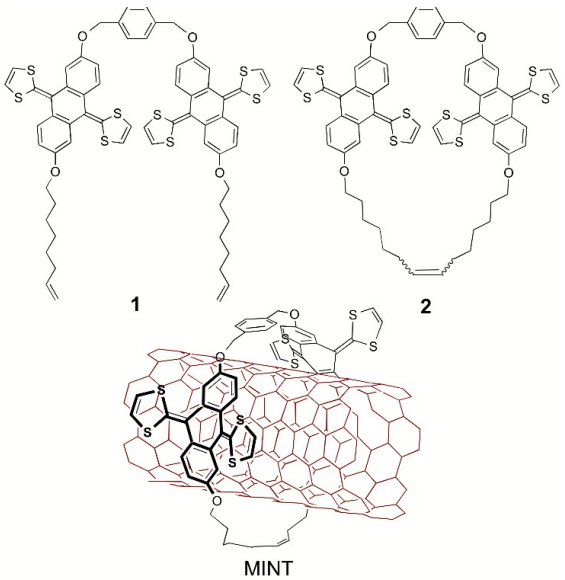

Fig. 1. Structure of U-shape **1**, macrocycle **2** and schematic representation of the structure of MINTs.

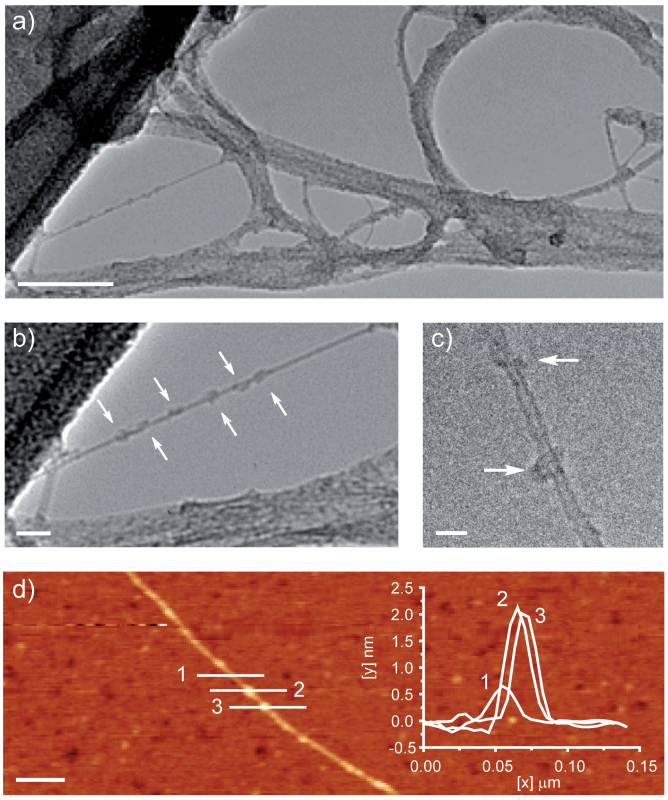

Fig. 2. a-c) Transmission electron micrographs (80 kV) of freestanding MINT$_{(6,5)}$-2 applied on a Lacey carbon/Cu film by drop casting from a suspension in methanol. d) AFM image of MINT$_{(6,5)}$-**2** sample deposited on mica substrate, showing a single SWNT with two macrocycles and height profiles across the nanotube (1) and the macrocycles (2 and 3). Scale bars are 50 nm for (a), 10 nm for (b), 2 nm for (c), and 100 nm for (d).

Firstly, we characterized our samples by transmission electron microscopy (TEM). To that end, the samples were dispersed in methanol by using ultrasonication for 10 min. The sample dispersions were then applied onto Lacey-carbon grids by the suction method. Throughout the scanned areas, large bundles of SWNTs, on one hand, and individualized SWNTs wrapped with objects of appropriate size and shape to be identified as macrocycle **2**, on the other hand, were noted. Representative images are shown in Figure 2, where several individual macrocycles are highlighted with white arrows. The micrographs are therefore in perfect agreement with the formation of MINT$_{(6,5)}$-**2**. In contrast, pristine (6,5)-SWNTs show clean walls under TEM (see in the Supplementary Information). To complement the TEM microscopy characterization, we used atomic force microscopy (AFM). The samples were suspended in tetrachloroethane (TCE) by sonication for 1 hour and the suspension was spin coated over mica. Figure 2d shows a representative image, in which an individual SWNT that presents two objects with suitable height (ca. 2 nm, see calculations below) to be macrocycles around (and not on top of) the nanotube. As expected, AFM images of pristine (6,5)-SWNTs did not show any protuberances of this kind.
To investigate the influence of the mechanically bound macrocycle **2** on the electronic structure of SWNTs, we performed a series of comparative spectroscopic assays with

MINT$_{(6,5)}$-**2** and pristine (6,5) SWNTs, including steady state absorption and emission spectroscopy, Raman spectroscopy, and femtosecond transient absorption spectroscopy. To this end, complementary spectroscopic studies were conducted with the nanotube and MINT samples suspended in D_2O with the help of sodiumdodecylbenzenesulfonate (SDBS) as a surfactant. Additionally, we performed experiments with sodiumdodecylsulfate (SDS), which corroborate our SDBS findings and are presented in the Supplementary Information.

Steady state absorption spectra give rise to typical absorption features of S_{22} transitions in the visible and S_{11} transitions in the near-infrared region of the spectrum (Figure 3). For instance, prominent absorptions for (6,5) - SWNTs at 569 and 979 nm together with less-intense absorptions of (7,6) - SWNTs, at 647 and 1138 nm, are detected for the pristine nanotube sample. Although TEM micrographs corroborate the high degree of functionalization for MINT$_{(6,5)}$-**2**, the typical absorption of the exTTF chromophore is not noticeable, as we have previously observed.[63,64] The MINT$_{(6,5)}$-**2** spectrum failed to exhibit major changes as far as absorption maxima are concerned. Nevertheless, a slight broadening as well as an overall intensity decrease of the absorption features for MINT$_{(6,5)}$-**2** point to weak electronic interactions between the exTTF macrocycles and SWNTs in the ground state. Baseline correction and subsequent normalization of the absorption spectra of the nanotubes and MINT$_{(6,5)}$-**2** shed light onto intensity variations in the ratio between peaks of different SWNT chiralities. Upon normalizing the absorption relative to the 1138 nm intensity (Figure 3) the (6,5)-SWNT related absorption peak appears significantly weaker in MINT$_{(6,5)}$-**2** than in the pristine nanotubes. These observations point to a noticeable effect of the nanotube chirality on the electronic interactions in the MINT sample.

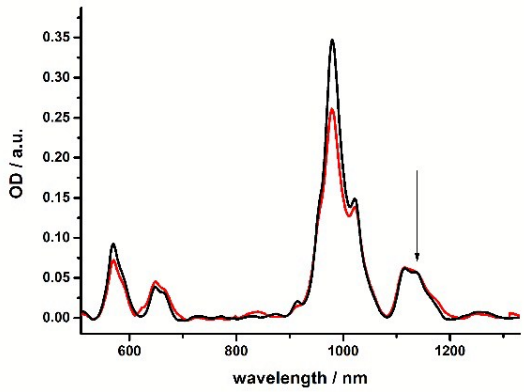

Fig. 3. Absorption spectra of (6,5)-enriched SWNTs (black) and MINT$_{(6,5)}$-**2** (red) in D_2O/SDBS (1 wt%) at room temperature – the spectra have been base-line corrected and normalized to the 1138 nm absorption.

In addition to absorption, fluorescence of the different samples was probed. Selective excitation with various wavelengths in a range between 530-800 nm leads to characteristic fluorescence features of (6,5), (8,4), (8,3), (7,5), and (7,6) SWNTs in the near-infrared region. Even at first glance, the 3D fluorescence maps of SWNTs and MINT$_{(6,5)}$-**2** reveal striking differences (Figure 4). In particular, appreciable fluorescence intensity variations are noted between the pristine and mechanically interlocked samples. The aforementioned is accompanied by a macrocycle-induced red shift of the fluorescence maxima from 986, 1121, 965, 1029 and 1130 nm in SWNTs to 991, 1127, 968, 1033 and 1133 nm in MINT$_{(6,5)}$-**2**.[64,66] The individual emission spectra, shown in the Supplementary Information, clearly demonstrate the selective fluorescence quenching of smaller diameter SWNTs such as (6,5), (8,3), and (7,5), when compared to the slightly larger (8,4) and (7,6), in line with our observations in absorption. Given the similar electronic nature of these chiralities, this selective quenching most likely stems from a higher degree of functionalization with macrocycle **2**.

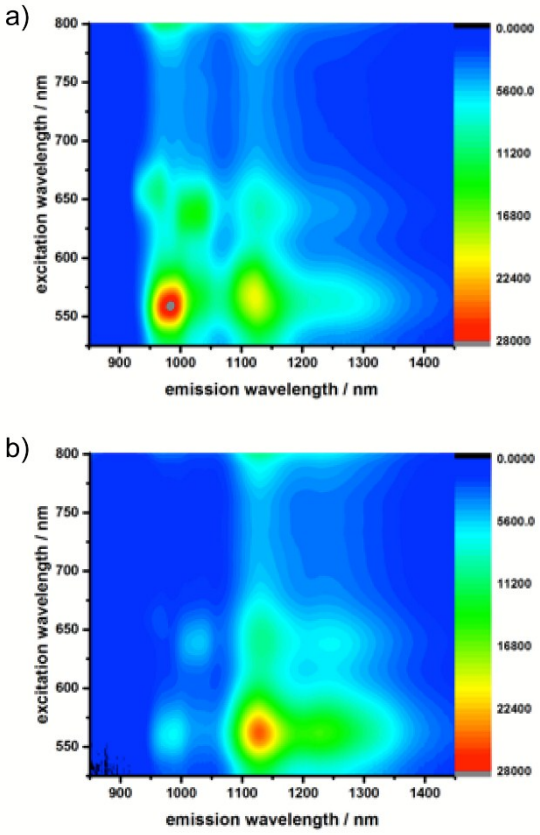

Fig. 4. 3D NIR fluorescence spectra of a) (6,5)-enriched SWNTs and b) MINT$_{(6,5)}$-**2** in D_2O/SDBS (1 wt%) measured with an OD of 0.35 at 570 nm.

We also recorded Raman spectra of SWNTs and MINT$_{(6,5)}$-**2** with λ_{exc} = 532, 785 and 1064 nm. The results are shown in Figure 5. The left panels of the figure show a comparison of the G-band of (6,5)-enriched SWNTs (black) and MINT$_{(6,5)}$-**2** (red), which reveals quantitatively small up-shifts for all three excitation wavelenghts, namely from 1573 to 1575, 1577 to 1582 and 1590 to 1591 cm^{-1}, respectively. This observation points to weak charge-transfer interactions between electron donating exTTF and SWNT in the ground state, and is in accordance with our previous observations.[66]

The size selectivity was investigated by careful analysis of the low frequency radial breathing mode (RBM) bands (Figure 5, right panels). For the on-resonance spectra, two RBMs were detected at 265 and 301 cm^{-1}, corresponding to (7,6) and (6,5)-SWNTs. When the Raman spectra are recorded with 1064 nm excitation, three main RBM features, at 268, 311, and 331 cm^{-1} originating from (7,6), (6,5), and (6,4)-SWNTs, respectively, were detected. When the spectra were normalized with respect to the (7,6)-RBM intensity, a noticeable decrease in the intensity of the RBMs corresponding to (6,5) and (6,4) SWNTs was observed in MINT$_{(6,5)}$-**2** (red) when compared to pristine nanotubes with all three excitation wavelengths. Although the Raman-based evidence is less compelling, the relative intensity decrease of the RBM features assigned to the smaller nanotubes is in line with the observations described for absorption and emission data. In summary, MINT-forming reaction favours functionalization of the smaller SWNTs diameter, in good agreement with theoretical predictions – vide infra.

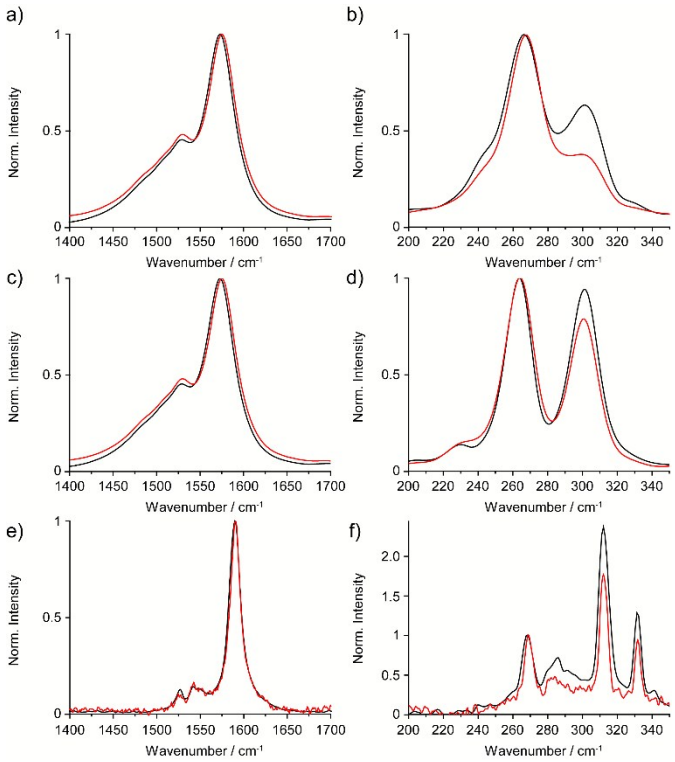

Fig. 5. Raman spectra (λ_{exc} = 532, 785 and 1064 nm from top to bottom) of SWNTs (black) and MINT$_{(6,5)}$-**2** (red). Left: Comparison of the G-band. Right: comparison of the RBMs.

To investigate the impact of the mechanically bound **2** on the excited state dynamics of SWNTs, we performed femtosecond transient absorption spectroscopic measurements. A set of transient absorption spectra of MINT$_{(6,5)}$-**2** with time delays from 0 to 500 ps are shown in Figure 6. The spectra are dominated by the instantaneously occurring ground state bleaching of the S_{11} transitions in the near infrared and the S_{22} transitions in the visible. The minima are located at 570, 648, 983, and 1121 nm. Features, which are assigned to excited state absorption, are found at 483, 531, 610, 711, 1072 and >1200 nm. In reference measurements with (6,5)-enriched SWNTs these features appear marginally blue-shifted. Considering the coverage in MINT$_{(6,5)}$-**2** in comparison to non-covalent SWNT hybrids, in which SWNTs are densely covered with exTTF, small shifts are likely to evolve.[67,69,70]

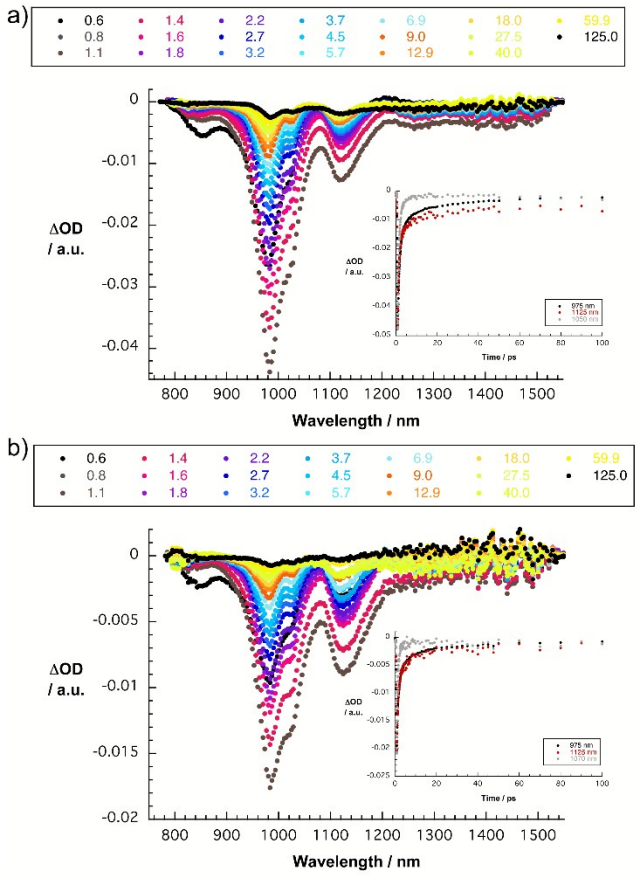

Fig. 6. Differential absorption spectra obtained upon femtosecond pump probe experiments (λ_{ex} = 387 nm) of a) (6,5)-enriched SWNTs and b) MINT$_{(6,5)}$-**2** in SDBS/D_2O (1wt%) with several time delays between 0.6 and 125 ps at room temperature.

More important are the differences in the temporal analyses of the excited state decays in MINT$_{(6,5)}$-**2** compared to the unfunctionalized SWNTs. For example, fitting the kinetic decay of the ground state bleaching of (6,5)-enriched SWNTs in SDBS, which give rise to the stronger fluorescence quenching, at 1000 nm yields three lifetimes of 230, 8, and 1 ps. The two shorter components are attributed to interband- or intertube charge carrier recombination, while the longer component is characteristic for the radiative exciton recombination. Notably, the lifetimes for MINT$_{(6,5)}$-**2** are drastically shortened compared to the values obtained in the SWNT reference, namely 80, 6, and 1 ps. In the insets of Figure 6, representative time profiles taken at different wavelengths for MINT$_{(6,5)}$-**2** and pristine nanotubes are compared. Please note that features of the one electron oxidized exTTF appear as a rather broad positive absorption at ~680 nm.[67,71] In MINT$_{(6,5)}$-**2**, this wavelength range is, however, dominated by ground state bleaching of SWNT related S_{22} transitions. A weak positive

signal at 700 nm is discernable and taken as evidence for the exTTF oxidation (see the Supplementary Information). In terms of SWNT reduction, we turn to the 1200 to 1600 nm range, where the broad and positive absorption is in line with spectroelectrochemical reduction of SWNTs. Based on this spectroscopic comparison we postulate that photoexcitation of MINT$_{(6,5)}$-**2** is followed by charge separation – 6 ps – affording a metastable charge separated state. Charge recombination – 80 ps – leads to the population of the ground state.

Turning to the weakly quenched fluorescent MINT$_{(7,6)}$-**2** fit at 1130 nm the kinetics are 270, 8, and 1 ps in comparison to 350, 12, and 1 ps obtained in the reference measurements with unfunctionalized SWNTs in SDBS. Thus, relative to the shortening of the lifetimes observed with the smaller (6,5)-SWNTs, the impact on the larger (7,6)-SWNTs is less pronounced.

A fair comparison of the photophysical properties of the supramolecular complexes SWNT + **2** vs. MINT$_{(6,5)}$-**2** was prevented by the insolubility of macrocycle **2** in aqueous solutions. However, this observation further confirms the mechanical link between the nanotubes and **2** in MINT$_{(6,5)}$-**2**, which allows for the solubilization of the non-polar **2** in water. Such radical changes in solubility are one of the earliest and most frequent observations in the chemistry of MIMs, and are one of the fingerprints of the mechanical bond.[72]

To investigate the influence of the mechanical link on the redox properties of macrocycle **2**, we studied the electrochemical behavior of solutions/suspensions containing **1**, **2**, and MINT$_{(6,5)}$-**2**, as well as mixtures of **1** or **2** with (6,5)-SWNT with identical loading of exTTF material. In particular, we used 0.34 mg/mL of MINT$_{(6,5)}$-**2** suspended in 0.1 M TBAP/DMF (TBAP = tetrabutylammonium perchlorate). In this case, the use of an organic solvent allows for comparison of the mechanically interlocked sample with the relevant supramolecular associates. In particular, we utilized SWNT + **1** and SWNT + **2** mixtures composed of 0.34 mg/mL of SWNT and 0.16 mg/mL of either **1** or **2**, which were also suspended in 0.1 M TBAP/DMF. As references, U-shape and macrocycle measurements, 0.16 mg/mL of either **1** or **2** were dissolved in 0.1 M TBAP/DMF. As shown in Figure 7, in all cases cyclic voltammograms show a reversible redox couple at around 0.26 V, which is ascribed to the two-electron oxidation/reduction of exTTF.[73,74]

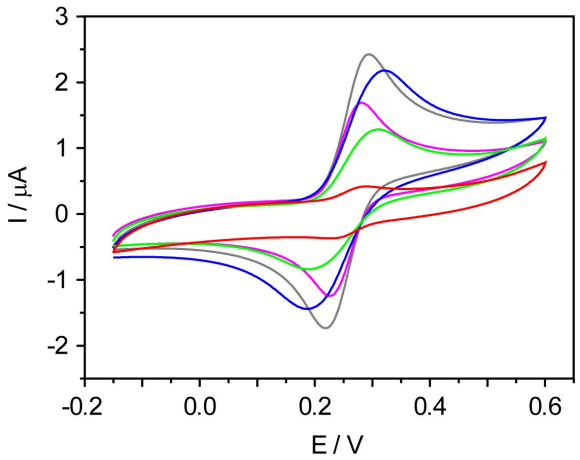

Fig. 7. Cyclic voltammetry (room temperature, 10 mV/s, 0.1 M TBAP in DMF, glassy carbon as working electrode, Pt wire as counter electrode, specific calomel electrode 1 M LiCl for organic media as reference electrode) of 0.16 mg/mL **1** (gray), and **2** (pink); 0.16 mg/mL **1** + 0.34 mg/mL (6,5)-SWNT (blue); 0.16mg/mL **2** + 0.34 mg/mL (6,5)-SWNT (green) and 0.34 mg/mL MINT$_{(6,5)}$-**2** (red).

Table 1. Anodic, cathodic, formal and peak potential separation extracted from the voltammograms of Fig. 7.

Sample	E_a/ mV	E_c/ mV	$E^{0'}$ / mV	ΔE_p /mV
1	291	221	256	70
2	315	195	255	120
1 + (6,5)-SWNT	279	28	254	51
2 + (6,5)-SWNT	303	198	251	105
MINTs$_{(6,5)}$-**2**	282	238	260	44

Table 1 shows the anodic (E_a) and cathodic (E_c) peak potentials, the formal potential ($E^{0'}$), as well as their separation ($\Delta E_p = E_c - E_a$) taken from cyclic voltammograms as shown in Figure 7. The first observation is that the formal potential remains basically invariable for all samples, which supports the lack of significant charge-transfer from exTTF to the SWNTs in the ground state, as observed in the absorption and Raman assays – vide supra. The exTTF oxidation/reduction becomes more irreversible for **2** relative to **1**. Upon mixing with SWNTs this tendency holds, but the peak separation is reduced for both species, which indicates a better electron transfer and a more reversible process thanks to the interactions with SWNTs. This effect is much stronger in MINT$_{(6,5)}$-**2**, indicating that there is a distinctive and more intimate interaction between the macrocyle and the nanotubes in the mechanically interlocked sample when compared to the **2** + SWNT supramolecular construct.

Moreover, different current intensities are observed for the different solutions/suspensions. The current intensities observed in the presence of the supramolecular models, **1** + SWNT and **2** + SWNT, are lower than those for **1** and **2** in the absence of the nanotubes. Considering that the concentrations of **1** and **2** were the same for all four samples (0.16 mg/mL), the current intensity is proportional to the square root of diffusion coefficient of each species. Thus, the lower diffusion coefficients of the mixtures with SWNTs, compared to that of pure **1** and **2**, suggests that there is a partial adsorption of the latter on the nanotube surface. In accordance with the observations on the peak potentials, the decrease in current

intensity is more evident in the case of MINT$_{(6,5)}$-**2**, again pointing to stronger interactions between the (6,5)-SWNTs and the macrocycles.

To study the consequences of this different interaction between SWNTs and the electroactive exTTFs in more detail, we have deposited equivalent amounts of the suspensions and solutions described above onto GC electrodes by drop casting. After drying in the dark – to avoid the photodecomposition of the electroactive molecule – under ambient conditions, the resulting modified electrodes were transferred to an electrochemical cell containing clean electrolyte (0.1M TBAP in DMF) and cyclic voltammograms at different scan rates were recorded. Figure 8 shows the results of these experiments. In all cases, the voltammograms show the typical shape of a surface-confined redox couple with small, although not zero, ΔE_p. They also show chemically reversible but electrochemically quasi-reversible charge-transfer kinetics for the exTTF/exTTF^{2+} couple (+0.2 V vs SCE), as indicated by their voltammetric wave-shape and changes in oxidative and reductive peak potentials (ΔE_p) as a function of sweep rate.

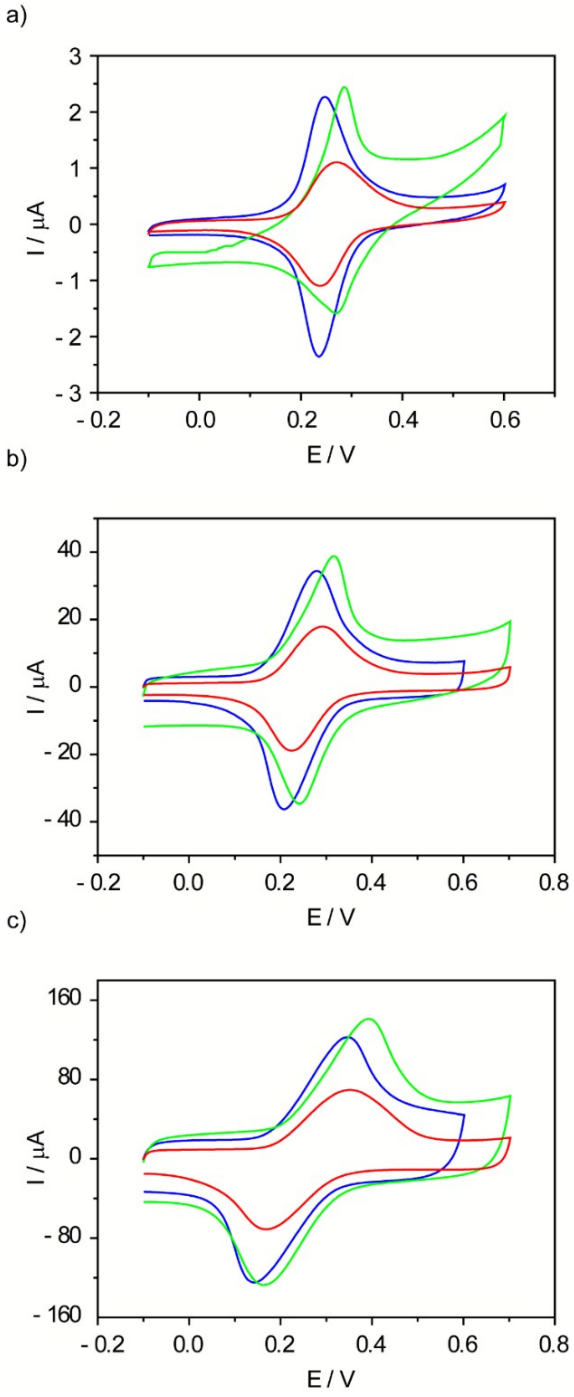

Fig. 8. Drop casting modified electrode with **1** + (6,5)-SWNT (blue), **2** + (6,5)-SWNT (green) and MINTs (red), electrochemical behavior in DMF/0.1M TBAP at (a) 10 mV/s, (b) 100 mV/s and (c) 500 mV/s.

The linear dependence of the anodic and cathodic peak currents (see the Supplementary Information) with the potential sweep rate also confirms that the redox couple is confined to the electrode surface.[75]

We performed Laviron analysis from the cyclic voltammetry of the three configurations shown in Figure 8 to assess how the presence of the mechanical bond in MINT$_{(6,5)}$-**2** affects the electron-transfer rates as compared to **1** or **2** when they are supramolecularly attached to the carbon nanotubes. The results are summarized in Figure 9.

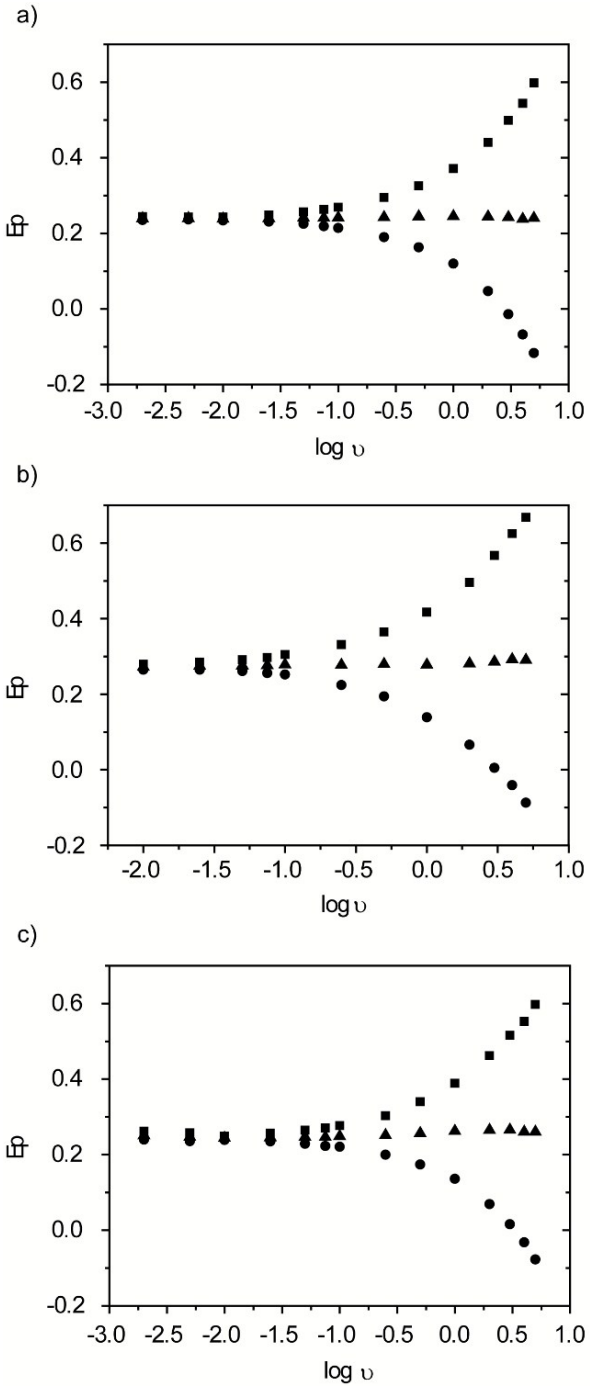

Fig. 9. Laviron plots of 6,5-SWNT+U-shape precursor (a) **1** + (6,5)-SWNT; (b) **2** + (6,5)-SWNT and (c) $MINT_{(6,5)}$-**2**; peak potentials at different scan rates (0.005 to 5 $V.s^{-1}$) on GC electrodes. (■) E_{an}-Oxidation peak potential, (●) E_{ca}- Reduction Peak Potential and (▲) $(E_{an}+E_{ca})/2$ formal potential.

In all cases, the peak potentials (E_p) in the anodic and cathodic scans converge to the values of the formal potential $E^{0'}$ at low scan rates (ν),whereas larger peak separations are observed at higher scan rates. The symmetry and the similar slopes in the linear parts of each plot for the anodic and cathodic branches suggest a transfer coefficient α of around 0.5. Analyses of the scan rate dependence yield significantly different charge-transfer rate constants for the MINT sample (21.4 s^{-1}) and the supramolecular models (26.1 s^{-1} for both **1** + (6,5)-SWNT and **2** + (6,5)-SWNT). Such differences confirm the fundamentally different type of interaction between the electroactive molecule and the carbon nanotube in the presence or absence of the mechanical bond, as they demonstrate a better disposition of the electroactive exTTF fragment to interact with the electrode surface in the case of the supramolecular models.

Finally, we have performed chronoamperometric measurements to quantify the diffusion coefficients of **1**, **2**, **1** + SWNT, **2** + SWNT, and MINTs, using a rotating disc/ring electrode (RRDE). Diffusion coefficients are a direct measurement of the size of the electroactive entity and, thus, any significant differences in the diffusion coefficient of **1** or **2** directly relate to their interaction with the SWNTs. Figure 10 shows the linear fits from chronoamperometric experiments at glassy carbon RRDE. We started recording the current intensity when the potential at the disc is competitive with the oxidation of exTTF. At this moment, exTTF is oxidized at both the disk and the ring. Consequently, the current intensity collected at the ring decreases, due to competitive processes. The time at which the current decreases (transit-time) is a function of the rotating rate, as explained in the Supplementary Information.[76,77] As the rotating rate (ω) increases, the oxidized species needs less time at the disc to arrive to the ring. In turn, fewer of the species to be oxidized reaches the ring electrode and the current intensity decreases.

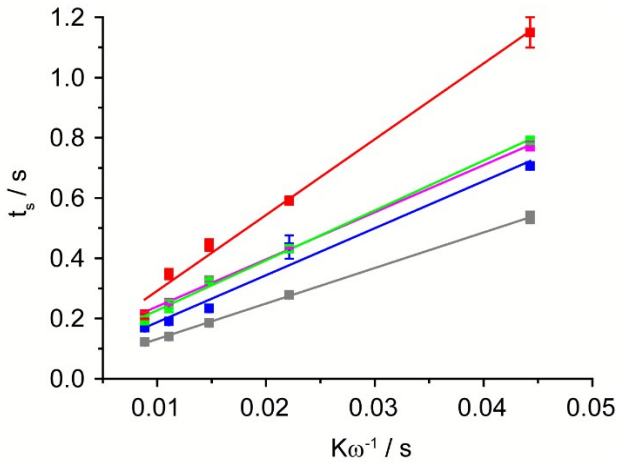

Fig. 10. Transit time (t_s) vs. $K\omega^{-1}$ plot enabling diffusion coefficient determination of **1** (gray), **2** (pink), **1** + (6,5)-SWNT (blue), **2** + (6,5)-SWNT (green) and (C) $MINT_{(6,5)}$-**2** (red).

In the absence of SWNTs, **1** and **2** show diffusion coefficients of 5.73 and 2.38 × 10^{-6} cm^2 s^{-1}, respectively. As expected, **1** shows a significantly larger diffusion coefficient, due to its quasi 1-D geometry in its extended configuration. Macrocycle **2**, on the other hand, is approximately disk-shaped. In the presence of SWNTs, the diffusion coefficient of **1** decreases significantly to 2.29 × 10^{-6} cm^2 s^{-1} as a consequence of its interaction with the carbon nanotubes. The tendency with **2** is the same, but quantitatively speaking the decrease is much smaller for **2** + SWNTs, for which a diffusion coefficient of 2.01 × 10^{-6} cm^2 s^{-1} was measured. Notably, the calculated diffusion coefficient is the average value of the diffusion coefficients of the electroactive species present in solution. A larger concentration of species bound to the carbon nanotube would

lead to a more pronounced decrease in the diffusion coefficients. Therefore, the experimental values reflect a more efficient interaction of **1** with SWNTs compared to **2**. Finally, MINT$_{(6,5)}$-**2** show a diffusion coefficient of 5.8 × 10^{-7} cm^2 s^{-1}, that is, a decrease of nearly one order of magnitude with respect to **1** and **2**. Such a pronounced decrease in the diffusion coefficient is yet one more proof of fundamentally irreversible interactions between the macrocycle and the carbon nanotube in MINTs. As macrocycles and SWNTs are mechanically interlocked in MINTs, no dissociation takes place, so the diffusion coefficient of the electroactive species approaches that of the larger nanotubes.

We have also modelled the MINTs at the Molecular Mechanics (MM) and Quantum Mechanical (QM) levels. For MM, we have used the MMFF94 force field to identify the SWNTs compatible with each macrocycle and facilitate the preparation of the experiments. Although we were mostly interested in a qualitative description of the bonding, we remained attentive to the limitations of this force field and only considered its results with an error bar of 10 kcal/mol, which is almost twice as much as its standard deviation with respect to ab initio calculations.[78] In this simplified description, if the diameter of the SWNT is smaller than the cavity of the macrocycle, its wall will have a small attractive effect on the molecule. The equilibrium geometries show that the thinner the SWNT are the more the macrocycle tends to fold around it – as much as permitted by its own internal structure – and the more the alkyl chain spreads over the surface of the SWNT, establishing positive dispersion interactions. In this case, the closing of the ring around SWNTs is favored by a template effect, and the absolute limit corresponds to the smallest existing diameter of around 0.4 nm. However, if the SWNT diameter is larger than the cavity of the macrocycle, the closing of the ring will only occur within the flexibility limits of the alkyl chain. In turn, the interactions between the SWNT and the macrocycle become repulsive. To obtain the upper diameter limit, we optimized the geometry of the closed macrocycle around SWNTs of increasing diameters until their interaction energy reaches half the opposite of a C-H bond, namely 40 kcal/mol. This is meant to remain well below the limit of what would become covalent bonding between SWNTs and the macrocycle. Furthermore, we take this as the limit at which we cannot apply the force field anymore. Using these criteria, we define a favourable region for the formation of MINTs and allow for the automatic screening of a broad range of SWNTs. The results for **2** are summarised in Figure 11 (full dataset and details can be found in the Supplementary Information). All SWNT chiralities presented in the sample are indeed found in the favourable diameter and energy ranges for the formation of the MINTs. In agreement with the absorption and Raman data, we observe that the smaller (6,5) SWNTs show significantly more favourable interaction energy than the larger (7,6), in particular, we have calculated −40 kcal/mol and −10 kcal/mol, respectively.

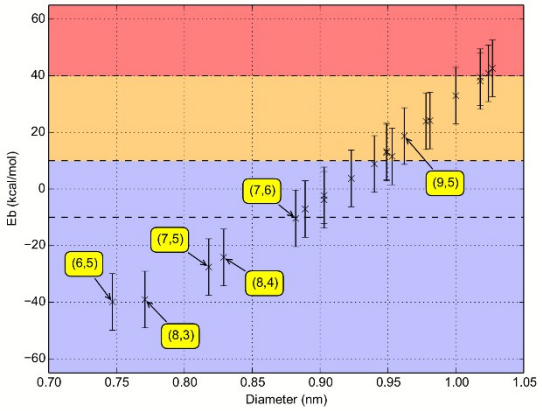

Fig. 11. Interaction energies of a series of SWNTs with macrocycle 2 (negative = attractive). Error bars of 10 kcal/mol have been represented for each combination. Blue: most favorable formation energy range. Orange: unfavorable formation energy range. Red: limit of the model. The SWNT chiralities observed experimentally have been labelled, as well as the largest diameter in the favourable area. The complete dataset is available in the supplementary material.

At the QM level, we have used Density Functional Theory (DFT) with a 6-31(d) Gaussian basis set and the PBE exchange-correlation functional, as implemented in the Gaussian 09 software package,[79] to model the charge transfer between **2** and a (6,5) SWNT. The results have been further processed with the VESTA software package.[80] Both molecules remain neutral, in agreement with the small charge-transfer interactions observed spectroscopically, with a very small overlap between a few hydrogen atoms of the alkyl chain of **2** and the SWNT. As shown in Figure 12a, the density overlap between the two components occurs at levels below 0.014 a.u. The weakness of their bonding is further confirmed by the contour plot in Figure 12b for low densities, where the contour slopes are extremely steep. The interaction of **2** with the SWNT is therefore based on dispersion interactions only, which opens up the intriguing possibility of **2** moving freely along the SWNT.[81]

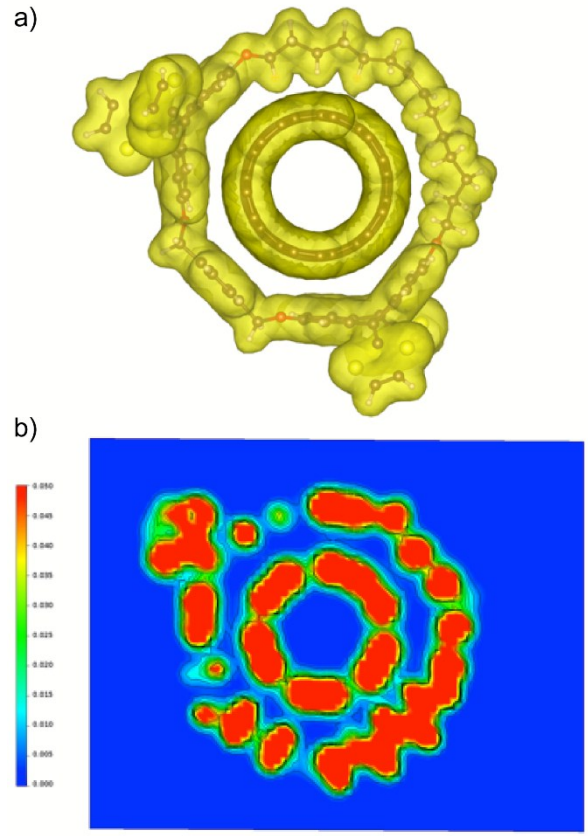

Fig. 12. a) Isosurface plot of the electronic density at 0.014 a.u., corresponding to the level where the intermolecular density bridges the SWNT and the macrocycle. b) Contour plot of the density from 0 (blue) to 0.05 a.u. (red) within the plane defined by the maximum intermolecular density.

Conclusion

This is the first report in which ample evidence for the influence of the mechanical bond on the properties of SWNTs is provided. Our results demonstrate that the formation of MINTs goes hand in hand with distinct effects on the carbon nanotubes, clearly different from what is found in non-interlocked supramolecular references.

In particular, we have described the synthesis and comprehensive characterization of MINTs based on (6,5)-enriched SWNTs and macrocycle **2**. TEM microscopy is consistent with the formation of rotaxane-type species. Raman, UV-vis-NIR absorption and vis-NIR steady state fluorescence indicate that the MINT-forming reaction is diameter-selective, which, together with the remarkable kinetic stability of MINTs,[3,64-66] suggests that mechanical interlocking could be a valuable strategy for the purification of complex mixtures of SWNTs. In the ground state, there is no significant charge-transfer between the electron donating exTTF and the SWNTs. However, in the excited state, transient absorption spectroscopy prompt to the efficient charge-transfer between the exTTF macrocycles as electron donors and SWNTs as electron acceptors.

The significantly different charge-transfer rate constants for MINTs and the supramolecular models confirm the different type of interactions between the exTTF and SWNT in the presence or absence of the mechanical bond. In addition, significant differences in the diffusion coefficients reflect irreversible interactions between the macrocycle and SWNT in MINTs.

From the multi-level theoretical description, we are able to preselect the best SWNT candidates for MINT functionalization and check the absence of covalent bonding between SWNTs and the macrocycles. The screening at the MM level can also be automated to accelerate the matching of SWNT-macrocycle pairs. As an add-on, the MM description is able to quickly provide relevant information about the overall flexibility of the macrocycles and has been used to eliminate precursors, which would be too rigid to close around SWNTs, before trying their synthesis experimentally.

Acknowledgements

A. dJ. and E.M.P. gratefully acknowledge funding from the European Research Council MINT (ERC-StG-2012-307609) and the MINECO of Spain (CTQ2014-60541-P). Y.P. and A.R. acknowledge financial support from the European Research Council (ERC-2010-AdG-267374), Spanish grant (FIS2013-46159-C3-1-P), Grupos Consolidados (IT578-13), and AFOSR Grant No. FA2386-15-1-0006 AOARD 144088, H2020-NMP-2014 project MOSTOPHOS, GA no. SEP-210187476 and COST Action MP1306 (EUSpec), as well as technical and human support provided by IZO-SGI SGIker of UPV/EHU and its European funding (ERDF and ESF). N. M. gratefully acknowledges financial support from the European Research Council ERC-2012-ADG-320441 (Chirallcarbon), MINECO of Spain (Grant Numbers CTQ2011- 24652 and PIB2010JP-00196), MOLESCO (Grant Number 606728), and CAM (FOTOCARBON Project S2013/MIT- 2841). N.M. is indebted to the Alexander von Humboldt Foundation. D.M.G. gratefully acknowledges funding from the Deutsche Forschungsgemeinschaft as part of the Collaborative Research Centre SFB 953 “Synthetic Carbon Allotropes” and of the Excellence Cluster “Engineering of Advanced Materials”. The Bayerische Staatsregierung is acknowledged for funding granted as part of the “Solar Technologies go Hybrid” initiative.

Notes and references

1 G. A. Breault, C. A. Hunter and P. C. Mayers, *Tetrahedron*, 1999, **55**, 5265-5293.
2 J. F. Stoddart, *Chem. Soc. Rev.*, 2009, **38**, 1802-1820.
3 A. de Juan and E. M. Pérez, *Nanoscale*, 2013, **5**, 7141-7148.
4 E. R. Kay, D. A. Leigh and F. Zerbetto, *Angew. Chem., Int. Ed.*, 2007, **46**, 72-191.
5 J. Berna, G. Bottari, D. A. Leigh and E. M. Pérez, *Pure Appl. Chem.*, 2007, **79**, 39-54.
6 C. Cheng, P. R. McGonigal, S. T. Schneebeli, H. Li, N. A. Vermeulen, C. Ke and J. F. Stoddart, *Nature Nanotech*. 2015, **10**, 547.
7 B. Lewandowski, G. De Bo, J. W. Ward, M. Papmeyer, S. Kuschel, M. J. Aldegunde, P. M. E. Gramlich, D. Heckmann, S. M. Goldup, D. M. D’Souza, A. E. Fernandes and D. A. Leigh, *Science*, 2013, **339**, 189-193.
8 H. Tian and Q.-C. Wang, *Chem. Soc. Rev.*, 2006, **35**, 361-374.

9 K. Zhu, C. A. O'Keefe, V. N. Vukotic, R. W. Schurko and S. J. Loeb, *Nature Chem*, 2015, **7**, 514-519.
10 E. A. Neal and S. M. Goldup, *Chem. Commun.*, 2014, **50**, 5128-5142.
11 R. Barat, T. Legigan, I. Tranoy-Opalinski, B. Renoux, E. Peraudeau, J. Clarhaut, P. Poinot, A. E. Fernandes, V. Aucagne, D. A. Leigh and S. Papot, *Chem. Sci.*, 2015, **6**, 2608-2613.
12 M. Franz, J. A. Januszewski, D. Wendinger, C. Neiss, L. D. Movsisyan, F. Hampel, H. L. Anderson, A. Görling and R. R. Tykwinski, *Angew. Chem., Int. Ed.*, 2015, **54**, 6645-6649.
13 L. D. Movsisyan, D. V. Kondratuk, M. Franz, A. L. Thompson, R. R. Tykwinski and H. L. Anderson, *Org. Lett.*, 2012, **14**, 3424-3426.
14 J. Winn, A. Pinczewska and S. M. Goldup, *J. Am. Chem. Soc.*, 2013, **135**, 13318-13321.
15 A. Fernandes, A. Viterisi, F. Coutrot, S. Potok, D. A. Leigh, V. Aucagne and S. Papot, *Angew. Chem., Int. Ed.*, 2009, **48**, 6443-6447.
16 J. M. Baumes, J. J. Gassensmith, J. Giblin, J.-J. Lee, A. G. White, W. J. Culligan, W. M. Leevy, M. Kuno and B. D. Smith, *Nature Chem*, 2010, **2**, 1025-1030.
17 E. M. Pérez, D. T. F. Dryden, D. A. Leigh, G. Teobaldi and F. Zerbetto, *J. Am. Chem. Soc.*, 2004, **126**, 12210-12211.
18 F. Cacialli, J. S. Wilson, J. J. Michels, C. Daniel, C. Silva, R. H. Friend, N. Severin, P. Samori, J. P. Rabe, M. J. O'Connell, P. N. Taylor and H. L. Anderson, *Nature. Mater.*, 2002,**1**, 160-164.
19 Q.-C. Wang, D.-H. Qu, J. Ren, K. Chen and H. Tian, *Angew. Chem., Int. Ed.*, 2004, **43**, 2661-2665.
20 A. Mateo-Alonso, C. Ehli, D. M. Guldi and M. Prato, *Org. Lett.*, 2013, **15**, 84-87.
21 A. Mateo-Alonso, C. Ehli, D. M. Guldi and M. Prato, *J. Am. Chem. Soc.*, 2008, **130**, 14938-14939.
22 V. N. Vukotic, C. A. O'Keefe, K. Zhu, K. J. Harris, C. To, R. W. Schurko and S. J. Loeb, *J. Am. Chem. Soc.*, 2015, **137**, 9643-9651.
23 K. Zhu, V. N. Vukotic, C. A. O'Keefe, R. W. Schurko and S. J. Loeb, *J. Am. Chem. Soc.*, 2014, **136**, 7403-7409.
24 V. N. Vukotic, K. J. Harris, K. Zhu, R. W. Schurko and S. J. Loeb, *Nature Chem.*, 2012, **4**, 456-460.
25 P. R. McGonigal, P. Deria, I. Hod, P. Z. Moghadam, A.-J. Avestro, N. E. Horwitz, I. C. Gibbs-Hall, A. K. Blackburn, D. Chen, Y. Y. Botros, M. R. Wasielewski, R. Q. Snurr, J. T. Hupp, O. K. Farha and J. F. Stoddart, *Proc. Natl. Acad. Sci. U. S. A.*, 2015, **112**, 11161-11168.
26 A. Coskun, M. Hmadeh, G. Barin, F. Gandara, Q. Li, E. Choi, N. L. Strutt, D. B. Cordes, A. M. Z. Slawin, J. F. Stoddart, J.-P. Sauvage and O. M. Yaghi, *Angew. Chem., Int. Ed.*, 2012, **51**, 2160-2163.
27 Q. Li, W. Zhang, O. S. Miljanic, C. B. Knobler, J. F. Stoddart and O. M. Yaghi, *Chem. Commun.*, 2010, **46**, 380-382.
28 Q. Li, C.-H. Sue, S. Basu, K. Shveyd Alexander, W. Zhang, G. Barin, L. Fang, A. Sarjeant Amy, J. F. Stoddart and M. Yaghi Omar, *Angew. Chem., Int. Ed.,* 2010, **49**, 6751-6755.
29 X.-Q. Wang, W. Wang, G.-Q. Yin, Y.-X. Wang, C.-W. Zhang, J.-M. Shi, Y. Yu and H.-B. Yang, *Chem. Commun.,* 2015, **51**, 16813-16816.
30 J. Wang and X. Zhang, *ACS Nano*, 2015, **9**, 11389-11397.
31 E. M. Peck, W. Liu, G. T. Spence, S. K. Shaw, A. P. Davis, H. Destecroix and B. D. Smith, *J. Am. Chem. Soc.*, 2015, **137**, 8668-8671.
32 C. Hu, Y. Lan, K. R. West and O. A. Scherman, *Adv. Mater.*, 2015, DOI: 10.1002/adma.201503844, Ahead of Print.
33 A. Goujon, G. Du, E. Moulin, G. Fuks, M. Maaloum, E. Buhler and N. Giuseppone, *Angew. Chem., Int. Ed*., 2016, **55**, 703-707.
34 A. Tamura and N. Yui, *Chem. Commun.,* 2014, **50**, 13433-13446.
35 H. W. Gibson, H. Wang, Z. Niu, C. Slebodnick, L. N. Zhakharov and A. L. Rheingold, *Macromolecules*, 2012, **45**, 1270-1280.
36 Z. Niu, F. Huang and H. W. Gibson, *J. Am. Chem. Soc.*, 2011, **133**, 2836-2839.
37 M. Lee, R. B. Moore and H. W. Gibson, *Macromolecules*, 2011, **44**, 5987-5993.
38 H. Dai, *Acc. Chem. Res.*, 2002, **35**, 1035-1044.
39 A. Jorio, G. Dresselhaus, M. S. Dresselhaus and Editors, *Carbon Nanotubes: Advanced Topics in the Synthesis, Structure, Properties and Applications. [In: Top. Appl. Phys., 2008; 111]*, 2008.
40 Z. Liu, S. Tabakman, K. Welsher and H. Dai, *Nano Res.*, 2009, **2**, 85-120.
41 N. Saito, Y. Usui, K. Aoki, N. Narita, M. Shimizu, K. Hara, N. Ogiwara, K. Nakamura, N. Ishigaki, H. Kato, S. Taruta and M. Endo, *Chem. Soc. Rev.*, 2009, **38**, 1897-1903.
42 J. M. Schnorr and T. M. Swager, *Chem. Mater.*, 2011, **23**, 646-657.
43 S. Park, M. Vosguerichian and Z. Bao, *Nanoscale*, 2013, **5**, 1727-1752.
44 D. Jariwala, V. K. Sangwan, L. J. Lauhon, T. J. Marks and M. C. Hersam, *Chem. Soc. Rev.*, 2013, **42**, 2824-2860.
45 H. Park, A. Afzali, S.-J. Han, G. S. Tulevski, A. D. Franklin, J. Tersoff, J. B. Hannon and W. Haensch, *Nature Nano*, 2012, **7**, 787-791.
46 A. D. Franklin, M. Luisier, S.-J. Han, G. Tulevski, C. M. Breslin, L. Gignac, M. S. Lundstrom and W. Haensch, *Nano Lett.*, 2012, **12**, 758-762.
47 C. Wang, D. Hwang, Z. Yu, K. Takei, J. Park, T. Chen, B. Ma and A. Javey, *Nature Mater.*, 2013, **12**, 899-904.
48 Q. Cao, S.-j. Han, G. S. Tulevski, Y. Zhu, D. D. Lu and W. Haensch, *Nature Nanotech.*, 2013, **8**, 180-186.
49 M. M. Shulaker, G. Hills, N. Patil, H. Wei, H.-Y. Chen, H. S. P. Wong and S. Mitra, *Nature*, 2013, **501**, 526-530.
50 P. Singh, S. Campidelli, S. Giordani, D. Bonifazi, A. Bianco and M. Prato, *Chem. Soc. Rev.*, 2009, **38**, 2214-2230.
51 M. Kanungo, H. Lu, G. G. Malliaras and G. B. Blanchet, *Science*, 2009, **323**, 234-237.
52 J. Zhao, Y. Gao, J. Lin, Z. Chen and Z. Cui, *J. Mater. Chem.*, 2012, **22**, 2051-2056.
53 J. L. Delgado, P. de la Cruz, F. Langa, A. Urbina, J. Casado, J. T. López Navarrete, *Chem. Commun*., 2004, 1734-1735.
54 R. Martín, F. J. Cespedes-Guirao, M. de Miguel, F. Fernández-Lázaro, H. García, A. Sastre-Santos, *Chem. Sci.,* 2012, **3**, 470-475.
55 Y.-L. Zhao and J. F. Stoddart, *Acc. Chem. Res.*, 2009, **42**, 1161-1171.
56 A. Wurl, S. Goossen, D. Canevet, M. Salle, E. M. Pérez, N. Martín and C. Klinke, *J. Phys. Chem. C,* 2012, **116**, 20062-20066.
57 S. D. Stranks, J. K. Sprafke, H. L. Anderson and R. J. Nicholas, *ACS Nano*, 2011, **5**, 2307-2315.
58 A. de Juan, A. López-Moreno, J. Calbo, E Ortí, E. M. Pérez, *Chem. Sci.* 2015, **6**, 7008-7014.
59 E. M. Pérez and N. Martín, *Org. Biomol. Chem.*, 2012, **10**, 3577-3583.
60 A. F. M. M. Rahman, F. Wang, K. Matsuda, T. Kimura, N. Komatsu, *Chem. Sci*., 2011, **2**, 862-867.
61 G. Liu, F. Wang, S. Chaunchaiyakul, Y. Saito, A. K. Bauri, T. Kimura, Y. Kuwahara, N. Komatsu, *J. Am. Chem. Soc.*, 2013, **135**, 4805-4814.
62 G. Liu, Y. Saito, D. Nishio-Hamane, A. K. Bauri, E. Flahaut, T. Kimura, N. Komatsu, *J. Mater. Chem.* A, 2014, **2**, 19067-19074.
63 F. Vialla, G. Delport, Y. Chassagneux, P. Roussignol, J. S. Lauret, C. Voisin, *Nanoscale* 2016, DOI: 10.1039/C5NR08023A

64 A. López-Moreno and E. M. Pérez, *Chem. Commun.*, 2015, **51**, 5421-5424.
65 A. de Juan, M. Mar Bernal and E. M. Pérez, *ChemPlusChem*, 2015, **80**, 1153-1157.
66 A. de Juan, Y. Pouillon, L. Ruiz-González, A. Torres-Pardo, S. Casado, N. Martín, Á. Rubio and E. M. Pérez, *Angew. Chem., Int. Ed.*, 2014, **53**, 5394-5400.
67 C. Romero-Nieto, R. García, M. Á. Herranz, C. Ehli, M. Ruppert, A. Hirsch, D. M. Guldi and N. Martín, *J. Am. Chem. Soc.*, 2012, **134**, 9183-9192.
68 E. M. Pérez, B. M. Illescas, M. Á. Herranz and N. Martín, *New J. Chem.*, 2009, **33**, 228-234.
69 C. Romero-Nieto, R. García, M. Á. Herranz, L. Rodríguez-Pérez, M. Sánchez-Navarro, J. Rojo, N. Martín and D. M. Guldi, *Angew. Chem., Int. Ed.*, 2013, **52**, 10216-10220.
70 V. Strauss, A. Gallego, G. de la Torre, T. W. Chamberlain, A. N. Khlobystov, T. Torres and D. M. Guldi, *Faraday Discuss.*, 2014, **172**, 61-79.
71 S. S. Gayathri, M. Wielopolski, E. M. Pérez, G. Fernández, L. Sánchez, R. Viruela, E. Ortí, D. M. Guldi and N. Martín, *Angew. Chem., Int. Ed.*, 2009, **48**, 815-819.
72 A. G. Johnston, D. A. Leigh, A. Murphy, J. P. Smart and M. D. Deegan, *J. Am. Chem. Soc.*, 1996, **118**, 10662-10663.
73 S.-G. Liu, I. Pérez, N. Martín and L. Echegoyen, *J. Org. Chem.*, 2000, **65**, 9092-9102.
74 M. R. Bryce and A. J. Moore, *Synth. Met.*, 1988, **27**, B557-B561.
75 R. H. Wopschall and I. Shain, *Anal. Chem.*, 1967, **39**, 1514-1527.
76 M. Chatenet, M. B. Molina-Concha, N. El-Kissi, G. Parrour and J. P. Diard, *Electrochim. Acta*, 2009, **54**, 4426-4435.
77 S. Bruckenstein and G. A. Feldman, *J. Electroanal. Chem.*, 1965, **9**, 395-399.
78 T. A. Halgren and R. B. Nachbar, *J. Comput. Chem.*, 1996, **17**, 587-615.
79 M. J. Frisch et al., Gaussian 09, Revision B.01, Gaussian Inc., Wallingford CT (2009).
80 K. Momma and F. Izumi, *J. Appl. Crystallogr.*, 2011, **44**, 1272-1276.
81 S. Freddi, L. D'Alfonso, M. Collini, M. Caccia, L. Sironi, G. Tallarida, S. Caprioli and G. Chirico, *J. Phys. Chem.*, 2009, **113**, 2722-2730.